Assessing Trajectory Accuracy of the CHCNAV RS10 Handheld Laser Scanner

Stefan Binapfl[1], Carolin Rünger[2], Gunnar Lelle-Neumann[1], Anette Eltner[2], Ferdinand Maiwald[1]

[1] Geodetic Institute, TUD Dresden University of Technology, 01069 Dresden, Germany –
(stefan.binapfl, gunnar.lelle-neumann, ferdinand.maiwald)@tu-dresden.de
[2] Institute of Photogrammetry and Remote Sensing, TUD Dresden University of Technology, 01069 Dresden, Germany –
(carolin.ruenger, anette.eltner)@tu-dresden.de

Keywords: Trajectory, accuracy, handheld laser scanning, personal laser scanning, CHCNAV RS10.

Abstract

Nowadays, an increasing number of handheld laser scanners with integrated Real Time Kinematic-Global Navigation Satellite System (RTK-GNSS) become available on the market. However, a method for determining their absolute trajectory accuracy remains difficult until now. Therefore, this study examines the absolute trajectory accuracy of a RTK-GNSS integrated handheld laser scanner under outdoor conditions. For this purpose, eight field measurements in different surrounding conditions were conducted and compared with a reference trajectory recorded using a total station in automatic target recognition (ATR) mode. The results of the field measurements demonstrate that the RTK- Personal Laser Scanner (PLS) achieves the manufacturer's specified absolute accuracy of 5 centimeters Root Mean Square Error (RMSE) in both the horizontal and vertical directions, despite slight shading caused through surrounding buildings or tree canopies. Larger deviations appeared particularly in areas with heavier shading from vegetation, for loop-free trajectories, and in environments with few features for Simultaneous Localization And Mapping (SLAM) optimization. In contrast, scans in structurally varied environments with clear geometric features, such as tree trunks, resulted in smaller deviations from the target trajectory, even though the scans were not taken under optimal GNSS conditions due to slight shading. Accordingly, while RTK-GNSS integration can enable centimeter-accurate positioning without any ground control points (GCP), factors such as route planning and environmental conditions still appear to be crucial to the absolute trajectory accuracy.

1. Introduction

The importance of PLS for three-dimensional (3D) data acquisition has increased significantly in recent years. While terrestrial laser scanning (TLS) remains preferred for high-precision applications, such as building deformation analysis or plant construction, due to its high measurement accuracy and lower systematic influences, PLS is increasingly becoming established in other fields of application. These include for example the documentation of cultural heritage, built environment and applications in forestry (Di Stefano et al., 2021).

A key advantage over static measurement methods is the high efficiency of data acquisition, especially in complex or difficult-to-access environments. In such scenarios, TLS would require a large number of scanning positions, which often leads to significantly longer measurement times (Oniga et al., 2021).

Current PLS systems are based on the integration of multiple sensors. These include an inertial measurement unit (IMU), which continuously measures the system’s rotational and translational movements, a Light Detection and Ranging (LiDAR) sensor for capturing the geometric structure of the environment, and additional camera sensors for obtaining visual feature information. The measured variables recorded by these sensors are fused together using a SLAM algorithm. The goal is to optimally combine all sensor data so that the scanner’s trajectory and the point cloud of the surrounding environment can be reconstructed in real time (Conti et al., 2024).

However, due to this sensor-based position determination, PLS systems are sensitive to systematical errors that can accumulate during measurement. As a result, the reconstructed trajectory of the scanner may deviate from the actual position due to drift effects. These deviations can result from the measurement uncertainties of the IMU as well as from the insufficient structural features of the environment. An established method for reducing these effects is loop closure, in which areas that have already been captured are revisited. By comparing redundant observations, the trajectory can be optimized subsequently and the drift effects are reduced. However, this procedure extends the recording time, as certain areas have to be captured multiple times (Cadena et al., 2016).

Another way to minimize drift errors in outdoor applications is to integrate RTK-GNSS. This satellite based integration has already been used for several years in other mobile measurement systems, such as mobile mapping or Unmanned Aerial Vehicle (UAV)-based laser scanning systems. In addition to continuously correcting IMU-based position estimates, RTK-GNSS also enables the recorded measurement data to be directly transformed into a higher-level geodetic coordinate system without using GCP as targets (Li et al., 2024).

The CHCNAV RS10 is one of the first handheld PLS systems to also include an integrated RTK-GNSS module into the SLAM algorithm. Unlike backpack-based PLS systems, where the GNSS antenna is attached externally, the RS10 has it integrated directly into the sensor system above the LiDAR unit. By using RTK-GNSS with real-time corrections from a network of reference stations, the captured point clouds can be immediately georeferenced and transformed into a higher-level coordinate system. In addition, continuous satellite-based positioning enables ongoing correction of the trajectory during data acquisition, which can significantly reduce drift errors in outdoor measurements. The integration of GNSS-based observations also eliminates the need for targeted loop closure within the trajectory, enabling loop-free scans, since the drift effects are corrected by satellite-based measurements. This further increases the efficiency of the recording process (Shanghai Huace Navigation Technology Ltd., 2024).

The aim of the article is to develop a method for investigating the absolute trajectory accuracy of PLS. For this purpose, the position deviation of the CHCNAV RS10 trajectory during outdoor scans is analyzed and evaluated.

This contribution has been peer-reviewed.
https://doi.org/10.5194/isprs-archives-XLIX-B1-2026-129-2026 | © Author(s) 2026. CC BY 4.0 License.

2. Related Work

Previous studies investigating the accuracy of PLS systems have mostly been based on comparing the resulting point clouds with a reference or target model. In this context, the accuracy of handheld laser scanners is often assessed using cloud-to-cloud or cloud-to-mesh comparisons (Gharineiat et al., 2024, Chudá et al., 2024, Urban et al., 2024, Martienßen, 2019, Blaskow & Eltner, 2023).

For example, Gharineiat et al. (2024) investigated the measurement accuracy of the mobile SLAM scanners NavVis VLX and Leica BLK2GO in indoor and outdoor areas. The point clouds were validated by comparing them with reference data collected using a total station and a static terrestrial laser scanner. The results show that accuracy is significantly dependent on the respective operating environment. While an average RMSE of approximately 5 millimeters was achieved indoors, the deviations outdoors ranged between 10 and 60 millimeters. Furthermore, the analysis showed that data quality is significantly influenced by walking speed and the selected trajectory. In particular, the use of loop closures has a positive effect on the quality of the results. At the same time, the authors highlight the time efficiency of mobile laser scanners compared to static measurement systems, as both indoor and outdoor surfaces can be captured within a few minutes. Chudá et al. (2024) assessed the accuracy of determining tree positions in different forest structures using the handheld laser scanners GeoSLAM ZEB Horizon and Stonex X120GO. The evaluation was carried out on five test areas with different tree species and varying stand densities, using a total station as a reference system to determine tree positions. The results of the study showed an average RMSE of 17.91 centimeters for the GeoSLAM scanner, while the Stonex scanner achieved an RMSE of 17.33 centimeters. Significant influences on accuracy were found in particular in the stock density and tree species. This study also highlighted the significant advantage of fast data acquisition, which makes PLS systems fundamentally suitable for deriving forestry parameters. Urban et al. (2024) investigated the accuracy of the SLAM scanner GeoSLAM ZEB Horizon using a 133-meter bridge as an example. The measurements of a terrestrial laser scanner and a total station served as references for the investigation. The results showed that the deviations from the reference measurements were in the lower centimeter range. Since PLS systems suffer from increased noise and systematic error influences, they are only suitable for high-precision building monitoring to a limited extent. At the same time, the authors also emphasized in this study the considerable time advantage of data acquisition compared to static laser scanners. Martienßen (2019) evaluated the potential applications and accuracy of the GeoSLAM ZEB-REVO in a mine. The assessment was conducted by comparing the generated point clouds with reference data from a terrestrial laser scanner and with target coordinates from previously determined polygon networks. The results of the study showed that the point clouds can contain significant deviations, particularly in extensive and geometrically homogeneous sections. Deviations of several decimeters were found at individual reference points. The author identified the main causes of these errors as the lack of sufficiently structured environmental features, which are necessary for the stable functioning of the SLAM algorithm, and drift effects of the IMU. The drift effects become more pronounced with increasing length of the measurement section, resulting in significantly greater deviations for a trajectory length of approximately 250 meters. Blaskow & Eltner (2023) investigated the suitability of PLS for the geometric mapping of small-scale environments using urban waterbodies as an example. The results of the study show that handheld laser scanners are generally suitable for the geometric capture of such scenarios. At the same time, it is emphasized that the length and duration of individual measurements should be adapted to the respective complexity of the environment to ensure accurate trajectory estimation. Furthermore, it is shown that good accuracies can be achieved for shorter trajectories compared to reference measurements using TLS. In addition, the authors demonstrate that the inclusion of control points distributed along the measurement object contributes to a significant improvement in georeferencing and thus in the overall accuracy of the PLS data.

With regard to evaluating handheld laser scanners, the quality of the trajectory, which strongly influences the overall precision of the point clouds, has often been neglected in the past. Against this background, the present study investigates the trajectory performance of the CHCNAV RS10.

3. Materials and Methods

This study analyzes the trajectory accuracy of the CHCNAV RS10 (Fig. 1) in outdoor scenarios. The CHCNAV RS10 is a handheld laser scanner whose operating principle, as with conventional PLS systems, is based on a combination of an IMU sensor, a rotating LiDAR unit with 16 channels and three additional cameras. The fusion of this sensor data enables continuous position and location determination during movement, allowing complex interior structures to be scanned within a few minutes.

Figure 1. CHCNAV RS10.

A key advancement of the RS10 over previous SLAM-based laser scanners is the integration of RTK-GNSS observations into the SLAM algorithm. This makes it possible to project the captured data outdoors directly into a higher-level coordinate system. According to the manufacturer, loop closures are no longer necessary for outdoor applications, as any drift errors are continuously corrected by satellite-based positioning. Furthermore, the manufacturer promises an absolute accuracy of 5 centimeters even if the GNSS signal is weak or lost for up to one minute using SFix technology. In this case, the trajectory is constructed on the basis of measurement data from the IMU, the LiDAR and the camera sensors exclusively. This makes it possible, to map indoor areas or underpasses within a higher-level coordinate system. Once these areas have been passed through and GNSS signals can be received, the trajectory of the PLS is additionally determined using satellite-based positioning again. Further technical specifications and information on device properties and accuracies are listed in Table 1.

Characteristic	Performance
Absolute accuracy	Horizontal: < 5 cm RMSE Vertical: < 5 cm RMSE
Relative accuracy	< 1 cm
Field of view	360° x 270°
Weight	1.9 kg
Channels	16
Range	0.05 – 120 m
GNSS-Systems	GPS, GLONASS, Galileo, BeiDou

Table 1. Technical specifications of CHCNAV RS10.

To evaluate the absolute accuracy, which the manufacturer specifies as 5 centimeters RMSE in the horizontal and vertical components, a Leica 360° prism was mounted on the top of the PLS instrument and continuously tracked by a Leica TS60 in ATR mode. In ATR mode, the TS60 provides an angular accuracy of 0.15 milligons in both the horizontal and vertical angles, and is therefore regarded as an instrument of superior accuracy suitable for evaluating the trajectory accuracy. Previous test measurements showed that the reference point of the CHCNAV RS10 trajectory is decentralized in the handheld laser scanner. The technical drawings provided by the manufacturer clearly confirmed this decentralized position.
Based on the drawings, a special construction was designed and 3D printed in which the prism is positioned vertically above this reference point of the trajectory. This ensured that the trajectory reference point of the RS10 and the center of the prism coincided in terms of position.
The remaining vertical offset was taken into account in the total station measurement. For this purpose, a corresponding prism height was entered for each observation, which corresponded to the height offset caused by the in-house design.
A Leica AP20 inclinometer was used to additionally account for device-related inclinations of the CHCNAV RS10. This ensured that both the RS10 trajectory and the measurements of the Leica TS60 were referenced to the same reference point independently of inclination. Due to this construction, no further consideration of the lever arm between the RS10 and the 360° prism was necessary. A representation of the construction used can be seen in Figure 2.

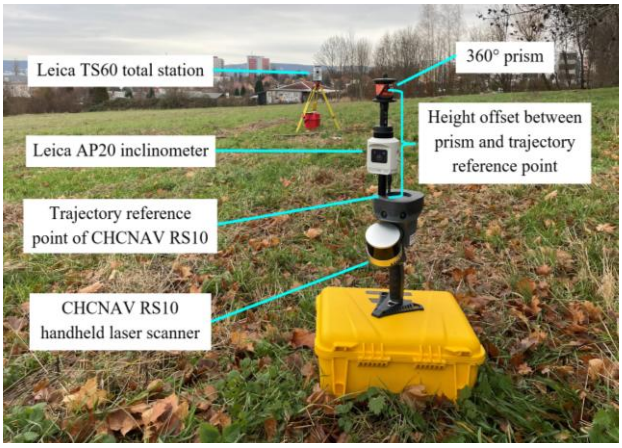

Figure 2. Construction for the 360° prism and Leica AP20 inclinometer.

4. Practical work

4.1 Laboratory experiments

Before conducting the field measurements, a laboratory experiment was necessary to confirm the accuracy and usability of our special designed construction. For this purpose, two scans (see Figure 3 & 4) were carried out inside Dresden University of Technology. The CHCNAV RS10 was continuously tracked by the Leica TS60 using the ATR mode. The measurements acquired by the total station were performed within a defined local coordinate system. The PLS was integrated into this coordinate system through the use of ground control points, which enabled its georeferencing. The trajectory determined by the TS60 was used as a reference to which the trajectory of the RS10 was compared and evaluated in terms of accuracy.

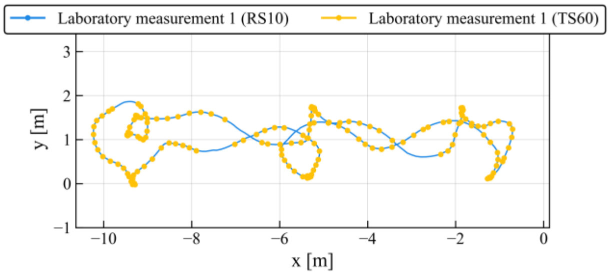

Figure 3. First laboratory experiment.

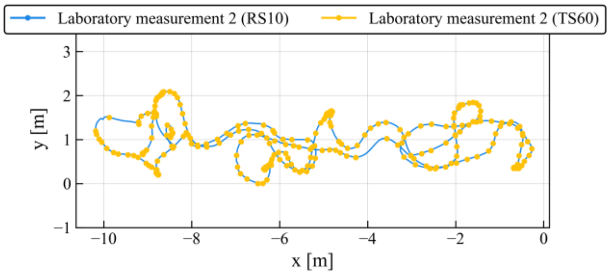

Figure 4. Second laboratory experiment.

The comparison of the trajectories was performed using the Python package Trajectopy (Tombrink et al., 2025). Before the actual calculation between the reference and the evaluated trajectory, it was necessary to convert both data sets to a uniform data basis. Due to the different sampling rates of approximately 210 Hz for the CHCNAV RS10 and approximately 3 Hz for the TS60 total station, it was necessary to synchronize the number of points. To achieve this, the trajectory data from the handheld laser scanner was reduced to the point density of the total station. This was done using the matching function implemented in Trajectopy. A nearest neighbor function based on Euclidean distances is used to identify corresponding point pairs between the two trajectories. In this way, each measurement point of the total station is assigned the spatially closest point of the RS10 trajectory. This procedure effectively resamples the trajectory of the RS10 to a sampling rate of approximately 3 Hz, so that both data sets have the same number of points and a consistent comparison calculation is possible.
On the one hand, the RMSE between the reference trajectory (TS60) and the evaluated trajectory (RS10) is calculated separately for the horizontal and vertical components. On the

https://doi.org/10.5194/isprs-archives-XLIX-B1-2026-129-2026 |

other hand, the standard deviation of the position deviations is used for further validation. The corresponding results are shown in Table 2.

Measurement	RMSE [mm]		Std.dev. [mm]
	Horizontal	Vertical	
Laboratory 1	6.4	2.8	4.2
Laboratory 2	7.9	4.1	3.8

Table 2. Results of the laboratory measurements.

The results of both laboratory tests are at a comparable level. The RMSE of the horizontal component is approximately twice as large as that of the vertical component in both measurements. A potential cause for this is the combined measurement uncertainty of the Leica AP20 and the 360° prism used, which together have an accuracy of approximately 3 to 5 millimeters according to the datasheets. The AP20 in particular is characterized by a tilt-dependent deviation, which has a greater effect on the horizontal component than on the vertical one. The standard deviations of approximately 4 millimeters in each case also indicate that both measurement series are subject to comparable systematic error influences. Since the RMSE of the 3D coordinate in the laboratory tests was 7.3 and 9.0 millimeters, respectively, the selected measurement setup is suitable for validating the trajectory of the RS10 in outdoor environments.

4.2 Field measurements

The field measurements were carried out on an open field in Dresden. In the southern, eastern, and northwestern parts of the measurement area, the GNSS signal was affected by shadows. These were caused by trees and surrounding buildings.
The Leica TS60 total station, serving as the ground truth measurement, was integrated into a GNSS-based control point network using free stationing. A total of seven GCPs were used for this purpose, with their coordinates determined by static GNSS observations. By integrating the total station into a control point network in the UTM Zone 33N coordinate system based on ETRS89, the measurement data of the TS60 is immediately available in the superior reference system.
The data acquisition with the CHCNAV RS10 was performed using RTK-GNSS, so these measurement data are also provided directly in the UTM Zone 33N / ETRS89 coordinate system. Consequently, the datasets from both measurement systems are located in the same reference system and can be compared directly without additional alignments.
The general measurement setup regarding the position of the total station, the spatial distribution of the GCPs, and the trajectory of the RS10 is shown schematically in Figure 5.

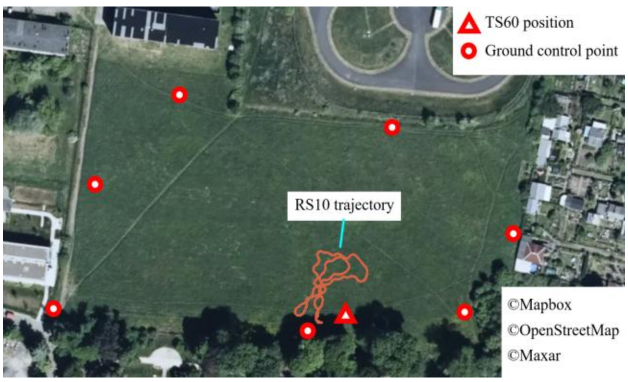

Figure 5. General measurement setup.

In total, eight separate scans were conducted. The corresponding trajectories of the individual measurements are shown in Figure 6.

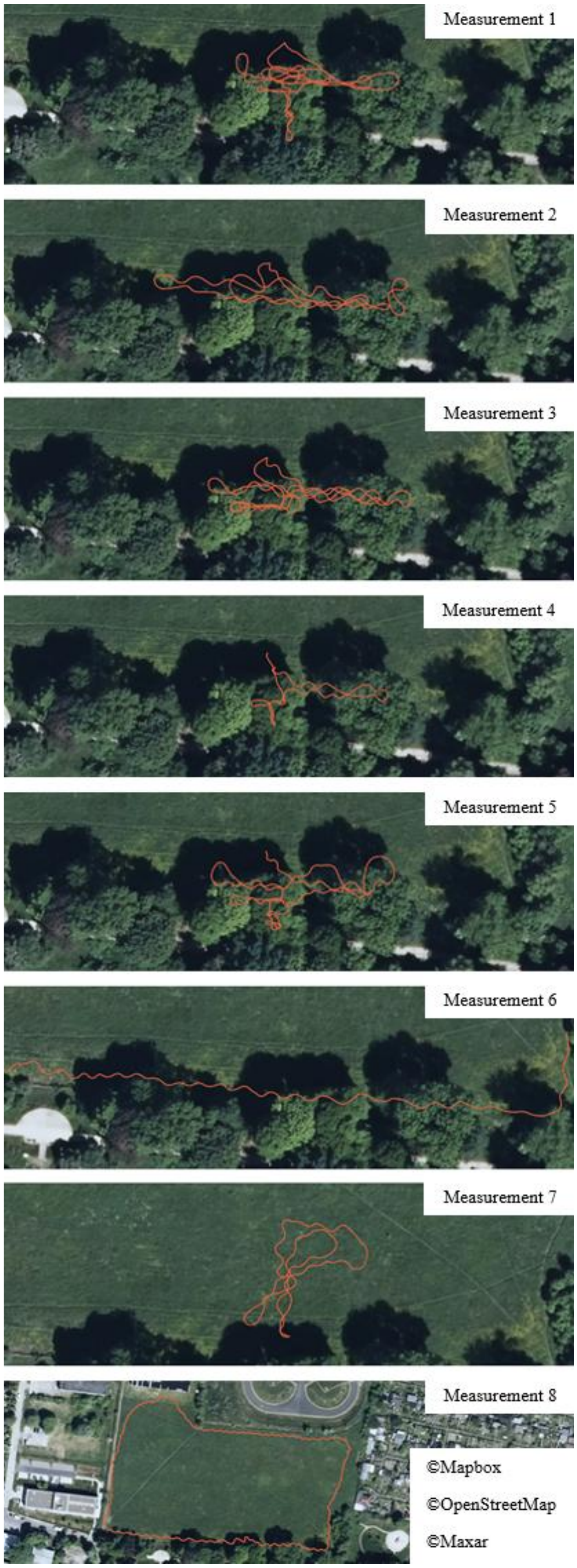

Figure 6. Trajectory paths of the scans.

https://doi.org/10.5194/isprs-archives-XLIX-B1-2026-129-2026 | © Author(s) 2026. CC BY 4.0 License.

The first five measurements were conducted under comparable conditions. All scans began in shadow-free conditions before the route led into the tree stand in the southern part of the study area. During the first measurement, the greatest amount of shading occurred due to a loop in the trajectory through dense tree cover, compared to scans 2 through 5.
The sixth measurement was conducted as a loop-free trajectory. The scan began west of the tree stand, then passed under the canopy, and finally ended east of the vegetation.
The seventh route was the only one in which no shading occurred during the entire measurement.
The eighth route covered the entire test field once. This resulted in the longest measurement time, with a scan duration of over eight minutes. The scan durations for all measurements are listed in Table 3.

Measurement	Scan duration [min]
1	4:38
2	3:49
3	4:34
4	1:31
5	3:43
6	2:27
7	2:51
8	8:16

Table 3. Scan durations of the field measurements.

For each scan, several parameters are recorded that potentially influence the accuracy of GNSS-based positioning. The most important parameters include the number of satellites used, ambiguity fixing and the horizontal dilution of precision (HDOP) value. To enable a comparison between the individual scans, the mean values for the number of satellites and the HDOP value were determined for the entire trajectory. For ambiguity resolution, the percentage of fixed rate within a scan was calculated. These parameters are listed in Table 4.

Measurement	Average number of satellites	Fixed rate [%]	Average HDOP
1	21.6	94.6	0.86
2	21.7	100	0.80
3	21.1	91.2	0.79
4	21.7	91.6	0.78
5	20.4	94.9	0.84
6	23.4	100	0.71
7	27.0	100	0.61
8	26.7	100	0.63

Table 4. Statistics of the field measurements.

Since the measurements from the CHCNAV RS10 and the Leica TS60 are provided in the same coordinate system, no additional alignment of the trajectories is necessary.
The workflow is therefore the same as that used in the laboratory comparisons. In the Trajectopy package, the trajectories of both devices were first matched and then compared. The measurements from the total station were again used as a reference, while the observations of the handheld laser scanner functioned as the data to be compared.

5. Results

In order to compare the absolute accuracy and quality of the individual scans, the deviation along the track is displayed for each trajectory, which is shown in Figures 7 to 14.

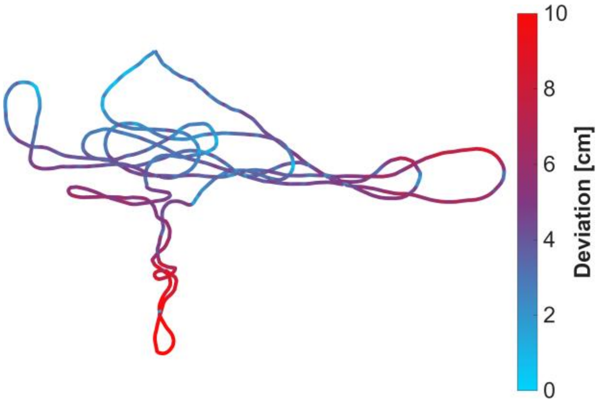

Figure 7. Absolute trajectory error of the first measurement.

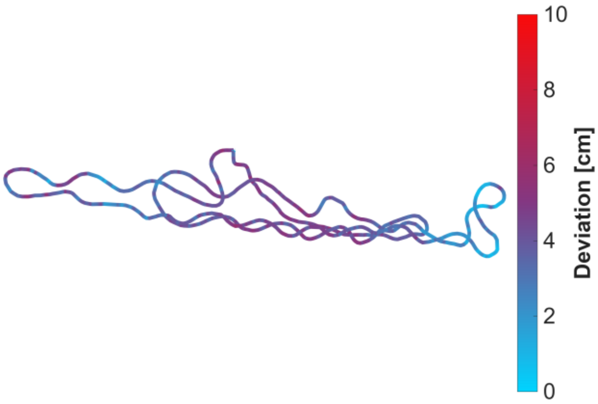

Figure 8. Absolute trajectory error of the second measurement.

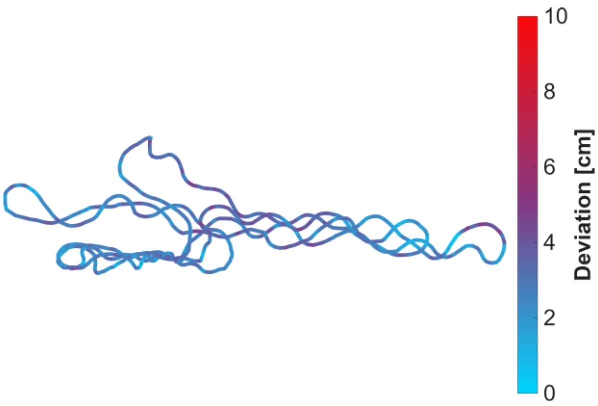

Figure 9. Absolute trajectory error of the third measurement.

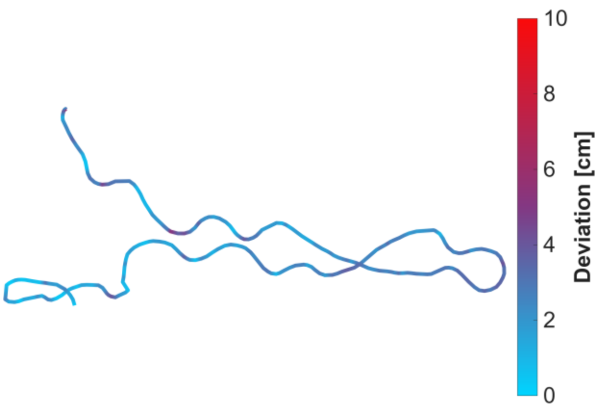

Figure 10. Absolute trajectory error of the fourth measurement.

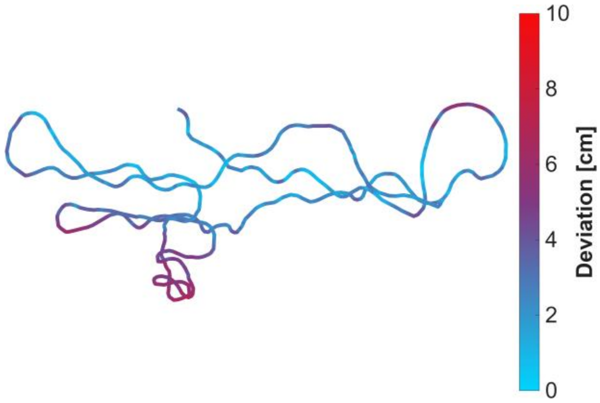

Figure 11. Absolute trajectory error of the fifth measurement.

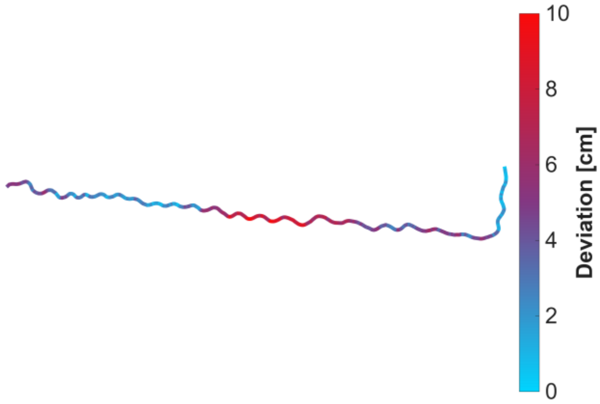

Figure 12. Absolute trajectory error of the sixth measurement.

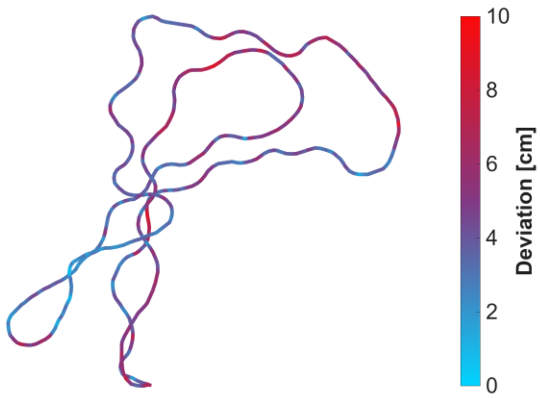

Figure 13. Absolute trajectory error of the seventh measurement.

Figure 14. Absolute trajectory error of the eighth measurement.

The first scan (Fig. 7) shows that the largest deviations from the total station's target trajectory are particularly noticeable in the southern loop. These deviations could be related to the dense tree population in this area, as shading from vegetation can potentially cause systematic influences. The remaining deviations along the trajectory are mainly in the range between 0 and 5 centimeters. In the second, third, fourth, and fifth measurements (Fig. 8-11), there are hardly no noticeable irregularities in the plots. These scans do not show any major maxima, so that almost all points have a deviation of less than 5 centimeters. The sixth scan (Fig. 12), which includes a loop-free trajectory, shows increased deviations in the path of movement, especially in the middle section. The seventh scan (Fig. 13), which was performed under open skies, shows deviations of about 5 centimeters for most of the points. A few deviations of up to 10 centimeters can be seen, which are marked by red areas in the plot. The last trajectory (Fig. 14) shows maximum deviations, particularly in the northeastern and northwestern sections of the curve. These could be due to multipath effects caused by the surrounding buildings.

Table 5 shows the percentage of points whose horizontal and vertical deviation is less than 5 centimeters of each scan.

Measurement	Percentage rate of horizontal deviation < 5 cm	Percentage rate of vertical deviation < 5 cm
1	90.7	85.7
2	99.1	99.9
3	99.9	100
4	99.2	100
5	99.1	95.4
6	70.2	100
7	84.8	98.9
8	88.8	94.1

Table 5. Percentage statistics of the field measurements.

The values shown in the table reflect the results of the plots considered above. In the first scan, the southern loop with the strongest shading causes the greatest deviations. These affect both horizontal and vertical accuracy. Accordingly, approximately 10% of the points in the horizontal component and around 15% of the points in the vertical component show a deviation of at least 5 centimeters.

As expected, scans 2 to 5 show the best results. In the horizontal position, all measurements show 99% of the points below a deviation of 5 centimeters. The picture is similar for the vertical component. Only in the fifth measurement do 4.6% of the points in the height component exceed a deviation of 5 centimeters.

In the sixth measurement, the deviations occur predominantly in the horizontal position. In the height component, on the other hand, all points are below a deviation of 5 centimeters.

The last two measurements show a similar pattern. In both cases, the horizontal accuracy is lower than the vertical accuracy. One possible reason for this could be the lower presence of distinctive features for the SLAM algorithm used compared to measurements 2 to 5.

The reason for the good results in measurements 2 to 5 could be that tree trunks and other objects in the environment served as useful features for the SLAM algorithm. Unlike the first scan, these measurements were only taken under slight shaded conditions, which may have had a positive effect on accuracy. The larger deviations in the last three scans may be related to the fact that no loops were performed in the 6th and 8th measurements. On the other hand, there may have been too few or unsuitable features for effective SLAM optimization in the 7th scan. To compare the deviations of the individual scans and classify them in terms of overall accuracy, Figure 15 shows the error distributions of the horizontal and vertical RMSE.

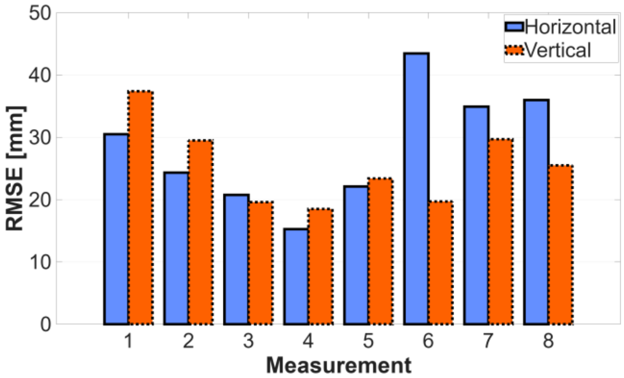

Figure 15. Horizontal and vertical RMSE of the field measurements.

Once again, this figure shows that the first and last three trajectories exhibit the greatest deviations. Nevertheless, the RMSE is less than 5 centimeters in both the horizontal and vertical directions in all trajectories. This means that the absolute accuracy of 5 centimeters RMSE in the horizontal and vertical directions specified by the manufacturer is maintained for every measurement.

6. Conclusion

This study successfully developed a method for the determination of absolute trajectory accuracy of PLS. The performed experiments investigated the absolute trajectory accuracy of a handheld laser scanner under RTK-GNSS-based outdoor conditions. In total, eight scans were performed and compared with a reference trajectory captured using a total station.

The results of the field measurements show that the absolute accuracy of the RS10 generally falls within the specifications provided by the manufacturer. For all scans performed, the RMSE values were below 5 centimeters in both the horizontal and vertical components, thus confirming the manufacturer’s specifications. At the same time, the results illustrate that trajectory accuracy is significantly influenced by the respective environmental and measurement conditions. Increased deviations occurred particularly in areas with greater shading from vegetation, for loop-free trajectories, and for scans with few distinctive environmental features for SLAM optimization. In contrast, measurements in structured environments, such as along tree trunks or building edges, showed noticeably more consistent and accurate results.

In summary, the studies demonstrate that RTK-GNSS-integrated PLS is able to achieve centimeter-level trajectory accuracy even under GNSS-based outdoor conditions. At the same time, it is evident that a suitable scan route and favorable environmental conditions are crucial for the quality of the results.

For future work, it would be useful to perform similar accuracy analyses in even more challenging areas for GNSS signals, such as in urban environments or complex forest structures. Furthermore, such studies should also be extended to other RTK-GNSS-based handheld laser scanners.

Acknowledgements

This work was funded by the project “Cross-border forest monitoring in the Bohemian Switzerland/Saxon Switzerland National Park” (TransForMon) (100736674) within the framework of the INTERREG Saxony – Czech Republic 2021-2027 programme, co-financed by the European Union through the European Regional Development Fund (ERDF). The project runs from 20 May 2024 to 31 December 2027, with EU funding (ERDF) amounting to 561,300.33€.

We would like to thank Vermessungstechnik Engelmann for providing the Leica AP20 inclinometer.

References

Blaskow, R., & Eltner, A. (2023). INVESTIGATION OF THE SUITABILITY OF A PERSONAL LASER SCANNING DEVICE FOR THE MONITORING OF SMALL WATER BODIES. *The International Archives of the Photogrammetry, Remote Sensing and Spatial Information Sciences*, *XLVIII-1/W1-2023*, 45–50. https://doi.org/10.5194/isprs-archives-XLVIII-1-W1-2023-45-2023

Cadena, C., Carlone, L., Carrillo, H., Latif, Y., Scaramuzza, D., Neira, J., Reid, I., & Leonard, J. J. (2016). Past, Present, and Future of Simultaneous Localization and Mapping: Toward the Robust-Perception Age. *IEEE Transactions on Robotics*, *32*(6), 1309–1332. https://doi.org/10.1109/TRO.2016.2624754

Chudá, J., Výbošťok, J., Tomaštík, J., Chudý, F., Tunák, D., Skladan, M., Tuček, J., & Mokroš, M. (2024). Prompt Mapping Tree Positions with Handheld Mobile Scanners Based on SLAM Technology. *Land*, *13*(1), 93. https://doi.org/10.3390/land13010093

Conti, A., Pagliaricci, G., Bonora, V., & Tucci, G. (2024). A COMPARISON BETWEEN TERRESTRIAL LASER SCANNING AND HAND-HELD MOBILE MAPPING FOR THE DOCUMENTATION OF BUILT HERITAGE. *The International Archives of the Photogrammetry, Remote Sensing and Spatial Information Sciences*, *XLVIII-2/W4-2024*, 141–147. https://doi.org/10.5194/isprs-archives-XLVIII-2-W4-2024-141-2024

Di Stefano, F., Chiappini, S., Gorreja, A., Balestra, M., & Pierdicca, R. (2021). Mobile 3D scan LiDAR: A literature review. *Geomatics, Natural Hazards and Risk*, *12*(1), 2387–2429. https://doi.org/10.1080/19475705.2021.1964617

Gharineiat, Z., Tarsha Kurdi, F., Henny, K., Gray, H., Jamieson, A., & Reeves, N. (2024). Assessment of NavVis VLX and BLK2GO SLAM Scanner Accuracy for Outdoor and Indoor Surveying Tasks. *Remote Sensing*, *16*(17), 3256. https://doi.org/10.3390/rs16173256

Li, Y., Feng, Q., Ji, C., Sun, J., & Sun, Y. (2024). GNSS and LiDAR Integrated Navigation Method in Orchards with Intermittent GNSS Dropout. *Applied Sciences*, *14*(8), 3231. https://doi.org/10.3390/app14083231

Martienßen, T. (Hrsg.). (2019). *Punktwolken von Handscannern und ihr Potenzial*. Wagner Digitaldruck und Medien GmbH. Geokinematischer Tag.

Oniga, V. E., Breaban, A. I., Alexe, E. I., & Văsii, C. (2021). INDOOR MAPPING OF A COMPLEX CULTURAL HERITAGE SCENE USING TLS AND HMLS LASER SCANNING. *The International Archives of the Photogrammetry, Remote Sensing and Spatial Information Sciences*, *XLIII-B2-2021*, 605–612. https://doi.org/10.5194/isprs-archives-XLIII-B2-2021-605-2021

Shanghai Huace Navigation Technology Ltd. (2024). *CHCNAV RS10—INNOVATIVE SURVEYING SLAM SOLUTION*.

Tombrink, G., Dreier, A., Klingbeil, L., & Kuhlmann, H. (2025). Spatio-temporal trajectory alignment for trajectory evaluation. *Journal of Applied Geodesy*, *19*(2), 321–331. https://doi.org/10.1515/jag-2024-0040

Urban, R., Štroner, M., Braun, J., Suk, T., Kovanič, Ľ., & Blistan, P. (2024). Determination of Accuracy and Usability of a SLAM Scanner GeoSLAM Zeb Horizon: A Bridge Structure Case Study. *Applied Sciences*, *14*(12), 5258. https://doi.org/10.3390/app14125258